

Does carbon dioxide pool or stream in the subsurface?

S. S. S. Cardoso* and J. T. H. Andres

*Department of Chemical Engineering & Biotechnology, University of Cambridge,
Cambridge CB2 3RA, UK*

*Electronic mail: ssscl@cam.ac.uk

PHYSICAL SCIENCES: Engineering Sciences, Applied Physical Sciences

Pools of carbon dioxide are found in natural geological accumulations and in engineered storage in saline aquifers. It has been thought that once this CO₂ dissolves in the formation water, making it denser, convection streams would transport it efficiently to depth, but this may not be so. Here, we assess the impact of natural chemical reactions between the dissolved CO₂ and the rock formation on the convection streams in the subsurface. We show that, while in carbonate rocks the streaming of dissolved carbon dioxide persists, the chemical interactions in silicate-rich rocks may curb this transport drastically and even inhibit it altogether. New laboratory experiments confirm the curtailing of convection by reaction. Wide and narrow streams of dense carbon-rich water are shut-off gradually as reaction strength increases until all transport of the pooled carbon dioxide occurs by slow molecular diffusion. These results show that the complex fluid dynamic and kinetic interactions between pooled carbon dioxide and the host rock may be limited to the shallower regions of the formation for hundreds to thousands of years. The deeper regions of the reservoir can remain virtually carbon free.

Keywords: Carbon dioxide, geochemistry, convection

Significance

Geological storage of anthropogenic carbon dioxide in subsurface aquifers has been proposed to reduce emissions into the atmosphere. A key challenge in the deployment of this technology is the long-term fate and safety of the stored carbon. A high efficiency of dissolution of the CO₂ in formation water has been attributed to convection streams driven by the relatively dense CO₂-rich brine. However, such arguments neglect the effects of geochemical reactions between the CO₂-rich, acidic brine and the porous rock. We show that for silica-rich rocks, natural geochemical reactions may disrupt the development of

convection, reducing drastically the transport of carbon dioxide to larger depths. Our work highlights the sensitivity of the efficiency of storage to the geochemistry of the reservoir.

A large natural flux of carbon occurs in the Earth's subsurface, taking a magnitude at a global scale of the order of 0.8 GtC/year (1). Contributing to this flux, and the carbon cycle, is the CO₂ transported from natural pools in a range of geological settings, particularly in sedimentary basins, intra-plate volcanic regions and in faulted areas (2). More recently, the geological storage of anthropogenic carbon dioxide in subsurface aquifers has been explored as a mitigation technique to reduce emissions into the atmosphere (2-8). An important challenge in the development of this technology is the behaviour and eventual fate of the stored carbon dioxide.

When relatively pure, either as a gas, liquid or in supercritical form, carbon dioxide is in general less dense than formation water and will therefore rise in the subsurface as a result of buoyancy forces. However, once it dissolves in the formation water, the mixture becomes denser. Thus, a dense boundary layer of carbon-rich water grows by diffusion (Figure 1). This layer may later become gravitationally unstable, breaking up into streaming currents that transport the CO₂-rich brine downward to increasing depths, while deeper formation water rises (9-11). Convection is a much more efficient and fast mode of transport than diffusion, inducing downward fluxes of carbon dioxide as large as 1 m³ per m² in a year, in a saturated rock with porosity of 0.1 and permeability of 10⁻¹³ m², for example. This mechanism of carbon transport has attracted much scientific attention in the context of geological storage, because it enhances the dissolution of the pooled carbon-dioxide and thereby increases the long-term stability and safety of storage. Experimental (12-16), theoretical (10,12,17,18) and numerical (10,19-22) studies have led to calculation of the time for onset of convection, the evolution of the thickness of the CO₂-rich layer and the dissolution rate of the CO₂ pool. Much less researched is the role of natural geochemical reactions between the CO₂-rich, acidic brine and the host rock on the dissolution and spreading of carbon dioxide in the subsurface. For example, the dissolution reaction between the acidic brine and a rock formation rich in calcium carbonate,

$$2\text{CaCO}_3(s) + \text{CO}_2(aq) + \text{H}_2\text{O}(l) \rightarrow \text{CO}_3^{2-}(aq) + 2\text{Ca}^{2+}(aq) + 2\text{HCO}_3^{2-}$$
, forms a solution denser than the acidic brine (1,23). This enhances convection and the transport of CO₂-rich brine to large depths in the medium. Conversely, a precipitation reaction such as that

between the acidic brine and a rock formation rich in calcium feldspar, $\text{CaAl}_2\text{Si}_2\text{O}_8(s) + \text{CO}_2(aq) + \text{H}_2\text{O}(l) \rightarrow \text{CaCO}_3(s) + \text{Al}_2\text{Si}_2\text{O}_5\text{OH}_4(s)$, promotes the precipitation of solids calcite and kaolinite, removing carbon dioxide from the liquid phase (1,23). Such reaction will attenuate convective motions. The impact of geochemical reactions such as these depends on the relative timescales for fluid motion, diffusion and reaction. Earlier work (24) suggested timescales of hundreds of years for convection, millions of years for diffusion; and weeks to centuries for slow and fast reactions, respectively (for a reservoir of depth 100 m and permeability 10^{-13} m^2). In the limit of very slow reactions, the geochemistry has little impact on fluid motion. However, intermediate and fast reactions may have a dramatic effect on the transport of the stored carbon dioxide. Previous numerical work (24-27) has indeed noted the possibility of a delay in the onset of convection caused by reaction, but has been unable to address the mechanisms by which reaction may stabilize convection. It has been assumed that, once initiated, convection continues indefinitely in an unbounded domain.

In this article, we consider a chemical reaction between the dissolved CO_2 and rock mineral M_1 (e.g., calcium feldspar) that removes carbon from the formation brine (23), reducing the mixture density, and thereby curbing the complex buoyant fingering. We show how such reaction can change profoundly the hydrodynamic behaviour of a diffusive layer of carbon dioxide and ultimately inhibit convection. To do so, we conduct a stability analysis of a transient diffusive layer undergoing a first-order, irreversible chemical reaction and compare the theoretical results with those of new laboratory experiments. We show here that the stability of a boundary layer depends crucially on how reaction constrains the wavelength of a random perturbation and on its effect on the diffusive concentration profile of the CO_2 .

The onset and shut-off of streaming

Consider an infinite, two-dimensional homogeneous porous medium where pure solute A overlies an aqueous layer (see Figure 1). A first-order reaction $A(aq) + M_1(s) \rightarrow M_2(s)$ occurs between the dissolved solute A and a chemical species in the porous solid M_1 , with reaction rate $k_r a [T^{-1}]$ per unit volume of fluid, where the solid-based kinetic rate constant is $k_r [mol \cdot L^{-2} T^{-1}]$ and the reactive surface area of the solid is $a [L^2 \cdot mol^{-1}]$. The system is described by the Darcy-Boussinesq equations (1)-(3) for the fluid velocity $\mathbf{v}' [LT^{-1}]$, the

reduced pressure $p' = P' - \rho_r g z' [ML^{-1}T^{-2}]$ and concentration of dissolved solute $C' [ML^{-3}]$ [3,17]:

$$\nabla' \cdot \mathbf{v}' = 0, \quad (1)$$

$$\mathbf{v}' = -\frac{k}{\mu} (\nabla p' - \rho_r \beta C' g \mathbf{i}), \quad (2)$$

$$\varphi \frac{\partial C'}{\partial t'} + \mathbf{v}' \cdot \nabla' C' = D \varphi \nabla'^2 C' - k_r a C'. \quad (3)$$

Here, the permeability of the porous medium $k [L^2]$ and the fluid viscosity $\mu [ML^{-1}T^{-1}]$ are constant. Density $\rho [ML^{-3}]$ is taken to depend linearly on C' as $\rho = \rho_r (1 + \beta C')$, where $\rho_r [ML^{-3}]$ is the reference density and $\beta [M^{-1}L^3]$ is the coefficient of density change due to concentration. The acceleration due to gravity is $g [LT^{-2}]$ and \mathbf{i} is the unit vector co-directional with the positive z -axis. Time is denoted by $t' [T]$. We note that when dissolution of the solute increases the density of the fluid, β is positive; reaction counteracts the dissolution effect on density by consuming solute, thereby having a stabilizing role on the diffusive layer for the configuration in Figure 1. Introducing the scales $L_c = \mu D \phi / (k \Delta \rho_0 g)$, $v_s = D \phi / L_c$, $t_s = L_c^2 / D$, $p_s = \mu D \phi / k$, and the solubility of the solute in the fluid C'_s , the governing equations are nondimensionalized, giving

$$\nabla \cdot \mathbf{v} = 0, \quad (4)$$

$$\mathbf{v} = -\nabla p + C \mathbf{i}, \quad (5)$$

and

$$\frac{\partial C}{\partial t} + \mathbf{v} \cdot \nabla C = \nabla^2 C - \frac{Da}{Ra^2} C. \quad (6)$$

Thus, the only parameter determining flow and transport in this system is a ratio of the Damköhler number and the square of the solutal Rayleigh-Darcy number,

$Da/Ra^2 = k_r a D \phi / (k \Delta \rho_0 g / \mu)^2$, which measures the relative magnitude between the timescale for onset of convection and the timescale for reaction. Thus, a small value of Da/Ra^2 reflects a slow reaction with little effect on the development of convection. Here, $\Delta \rho_0 = \rho_r \beta C'_s$ is the maximum density contrast between pure and solute-saturated fluid. The system (4)-(6), with initial condition $C_b(0, z) = 0$, far field condition $C_b(t, z \rightarrow \infty) = 0$ and interface condition $C_b(t, 0) = 1$, has a stagnant base state

$$C_b(t, z) = \exp\left(-\frac{\text{Da}}{\text{Ra}^2}t\right) \text{erfc}\left(\frac{z}{2\sqrt{t}}\right) + \frac{\text{Da}}{\text{Ra}^2} \int_0^t \exp\left(-\frac{\text{Da}}{\text{Ra}^2}s\right) \text{erfc}\left(\frac{z}{2\sqrt{s}}\right) ds \quad (7)$$

$$\mathbf{v}_b = 0, \quad p_b = p_b(z, t), \quad (8)$$

where $p_b(z, t)$ is the solution of Eq. (5) for the concentration profile in (7). Linearizing equations (4)-(6) around the base state (7)-(8), eliminating pressure and horizontal velocity, and expanding transverse perturbations into time-dependent Fourier modes as

$\{\hat{v}(x, \eta, t), \hat{C}(x, \eta, t)\} = \{v_0(\eta, t), C_0(\eta, t)\}e^{ikx}$ leads to,

$$\frac{1}{4t} \frac{\partial^2 v_0}{\partial \eta^2} - k^2 v_0 = -k^2 C_0 \quad (9)$$

$$t \frac{\partial C_0}{\partial t} = \left(\frac{1}{4} \frac{\partial^2}{\partial \eta^2} + \frac{\eta}{2} \frac{\partial}{\partial \eta}\right) C_0 - \left(k^2 + \frac{\text{Da}}{\text{Ra}^2}\right) C_0 t - \frac{v_0}{2} \sqrt{t} \frac{\partial C_b}{\partial \eta} \quad (10)$$

where $\eta = z'/(2\sqrt{t'})$ and k is the wavenumber in the horizontal x -direction. The boundary conditions are $v_0 = C_0 = 0$ at $\eta = 0, +\infty$. This initial value problem was solved numerically using the finite-element method in partial-differential-equation solver Fastflo (28). Test simulations were conducted to ensure that the results became independent of particular initial conditions well below the times for onset of instability and agreed with previously published solutions for the inert system (20). The concentration perturbation was measured using the norm $\bar{C}_0(t) = \int_0^{L_\eta} C_0(\eta, t) d\eta / L_\eta$, where L_η is the extent of the computational domain. The growth rate of this perturbation was defined as $\sigma = \ln[\bar{C}_0(t)/\bar{C}_0(t - \Delta t)]/\Delta t$.

Figure 2 shows the marginal stability curves ($\sigma = 0$) for different values of Da/Ra^2 . Inside each U-shaped or closed curve the diffusive layer is unstable to transverse disturbances ($\sigma > 0$), while in the outside region it is stable ($\sigma < 0$). The diffusive layer is stable at early times but at larger times there is a range of unstable modes, between a small and a large wavenumber cut-off. For the inert system ($\text{Da}/\text{Ra}^2 = 0$), the time for onset of convection is almost constant at intermediate values of k , owing to the stabilizing effect of vertical diffusion. Vertical diffusion has a relative maximum influence at small wavenumbers when transverse diffusion is negligible, leading to an increase in the time for onset of convection on the left side of the diagram. At high wavenumbers, transverse diffusion is dominant and

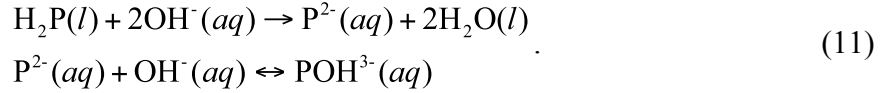
stabilizes the system. Reaction has a stabilizing effect on all wavenumbers, thereby increasing the time for onset of convection, and concomitantly causing an increase in the low wavenumber cut-off and a decrease in the high wavenumber cut-off, with a consequent narrowing of the window of instability. Crucially, as the destabilizing concentration gradient weakens with time, reaction can overcome its effect and stabilize the system after a finite period of convection, as reflected by the closed marginal curves. This finite period of growth of instability decreases as Da/Ra^2 increases until it disappears at the critical value $Da/Ra^2 = 2.69 \times 10^{-3}$, above which the system becomes unconditionally stable for all wavenumbers and times.

The maximum growth rates in Figure 3 exhibit a rapid increase at small times followed by a slower decay after the maximum. Reaction has two stabilizing effects: it reduces the concentration perturbation by consuming solute and it decreases the magnitude of the destabilizing base concentration gradient. These mechanisms have the largest joint effect on the most unstable wavenumber, causing a pronounced decrease in the maximum growth rate as strength of reaction rises. For the critical value of $Da/Ra^2 = 2.69 \times 10^{-3}$, all wavenumbers are stable. The most unstable wavenumber is independent of Da/Ra^2 and decreases gradually with time tending to an asymptotic value of $k = 0.05$. This temporal shift to lower wavenumbers is caused by the weaker effect of vertical diffusion compared to transverse diffusion as time progresses. Since reaction delays the onset of convection, the temporal shift in k causes a decrease in the wavenumber at onset of convection as reaction strength increases.

Laboratory Experiments

To validate our theoretical predictions, new laboratory experiments using an acid-base reaction in a Hele-Shaw cell were developed. Although the fingering of acid-base reactions has been studied before for immiscible (29,30) and miscible (31,34) layers, these systems cannot mimic the CO₂ problem described above, because either convection developed in both layers or reaction was limited to the surface between the two layers. To mimic the growing boundary layer of carbon dioxide, we devised a new reaction system in which a dense solute diffuses from the upper layer into an immiscible lower layer where it undergoes a first-order reaction. Experiments were performed in a Hele-Shaw cell with a layer of phenolphthalein dissolved in 4-methyl-2-pentanone (commonly known as methyl isobutyl

ketone or MIBK) overlying an aqueous solution of sodium hydroxide. Colorless phenolphthalein (H_2P) is instantaneously ionized in the presence of a strong base to form dark pink anion P^{2-} ; the anion then more slowly reacts with the strong base ($pH > 11$) to form the colorless carbinol POH^{3-} , according to (35),



When the concentration of base is much larger than the concentration of anion P^{2-} , the second step in the reaction is pseudo first-order with respect to the anion, with a rate constant proportional to the concentration of base (36). It may be shown that this step mimics the mineralization reaction for the carbon dioxide system in Figure 1, provided it is accompanied by a small density decrease and the concentration of POH^{3-} remains much smaller than the concentration of P^{2-} . Density measurements for reaction (11) in a well-mixed vessel connected to a capillary tube show that the former condition is satisfied, with

$\rho_r \beta C'_s \approx 0.17 \text{ kg/m}^3$ for a hydroxide solution with $14 < pH < 14.7$ and a concentration of phenolphthalein in MIBK of 1.74 g/dm^3 .

Figure 4 shows the evolution of the pink diffusive layer of P^{2-} as it grows into the underlying colorless hydroxide solution for three experiments with increasing values of Da/Ra^2 . The convective fingers develop earlier and descend into the underlying solution faster in the slowly reacting case A ($Da/Ra^2 = 5 \times 10^{-4}$, $t > 1.5 \times 10^2$) than for the intermediate reaction speed, case B ($Da/Ra^2 = 1 \times 10^{-3}$, $t > 2.9 \times 10^2$), while convection occurs only during a short period of time for the fast reaction in case C ($Da/Ra^2 = 2.7 \times 10^{-3}$, $3.4 \times 10^2 < t < 1.5 \times 10^3$), after which the boundary layer remains diffusive and confined to the top of the hydroxide layer. Gradual fading of the pink fluid is observed in all three cases at larger times, showing the progression of the second step in reaction (14). These experimental observations indicate both a delay of onset and a weakening of convection as Da/Ra^2 increases, thus supporting our earlier theoretical findings. The measured times for onset of convection are compared with the linear stability results in Figure 5, showing very good agreement. The very weak convection observed in case C is well reflected by the drastic curbing effect of reaction on the predicted maximum growth rate $\sigma_{\max kt}$ (over time and wavenumber). Also shown in Figure 5 is the onset time for the inert system consisting of acetic acid dissolved in MIBK overlying water. The wavenumber at the onset of instability is estimated for reactive case A to be $k \approx 0.03$,

which is significantly smaller than the theoretical value of 0.06 (Figure 3), owing to the merger of initial instabilities before they become visible.

The transport of carbon dioxide

A faster mineralization reaction between the CO₂ dissolved in brine and the surrounding rock matrix enhances the trapping of CO₂ in solid form, thus increasing its long-term retention in the subsurface. However, as shown above, reaction may also curb significantly the downward convective transport of CO₂ in the reservoir, retaining it at shallower depths. For example, chemical reaction between the acidic brine and a rock formation rich in calcium feldspar,

$\text{CaAl}_2\text{Si}_2\text{O}_8(s) + \text{CO}_2(aq) + \text{H}_2\text{O}(l) \rightarrow \text{CaCO}_3(s) + \text{Al}_2\text{Si}_2\text{O}_5\text{OH}_4(s)$, promotes the precipitation of calcite and kaolinite, removing carbon dioxide from the liquid phase and thereby reducing its density. Assuming the rock matrix has porosity of 0.1 and permeability of 10^{-13} m^2 , we estimate $\text{Da}/\text{Ra}^2 = 2.6 \times 10^{-3}$ (using kinetic data from (1)). Convection is predicted to initiate one month after injection of the carbon dioxide, with convection streams as wide as 4 m. However, these streams remain weak and completely shut-off after a short period of only two months. After this, the carbon dioxide will be transported by much slower diffusional processes. The results presented in this work have important practical implications for storage of carbon dioxide in saline aquifers, enabling informed screening of the most effective sites. Our results also aid the understanding of the natural flow of carbon dioxide in the subsurface and its contribution to the global carbon cycle. The work is of broader relevance for diffusive boundary layers in porous media encountered in other diverse fields, including enhanced oil recovery (37), geothermal systems (38), and pollution and brine migration in the subsurface (39).

ACKNOWLEDGMENTS

J. T. H. A. gratefully acknowledges the Schlumberger Foundation for financial support.

1. Marini L (2007) *Geochemical sequestration of carbon dioxide* (Elsevier).
2. IPCC (2005) *Special Report on Carbon Dioxide Capture and Storage*, edited by Metz B. *et al.* (Cambridge University Press, Cambridge, UK and New York, NY, USA).
3. Falkowski P, *et al.* (2000) The global carbon cycle: A test of our knowledge of earth as a system. *Science* 290:291–296.
4. Hoffert MI, *et al.* (2002) Advanced technology paths to global climate stability: Energy for a greenhouse planet. *Science* 298:981–987.
5. Lackner KS (2003) Climate change. A guide to CO₂ sequestration. *Science* 300:1677–1678.
6. Pacala S, Socolow R (2004) Stabilization wedges: Solving the climate problem for the next 50 years with current technologies. *Science* 305:968–972.
7. Orr FM, Jr. (2009) Onshore geologic storage of CO₂. *Science* 325:1656–1658.
8. Szulczewski ML, MacMinn CW, Herzog HJ, and Juanes R (2012) Lifetime of carbon capture and storage as a climate-change mitigation technology. *Proc Natl Acad Sci USA* 109(14):5185–5189.
9. Lindeberg E and Bergmo P (2003) The long-term fate of CO₂ injected into an Aquifer. In the 6th International Conference on Greenhouse Gas Control Technologies, Kyoto, Japan, 2002. Proceedings edited by J. Gale and Y. Kaya (Elsevier Science BV, Amsterdam).
10. Riaz A, Hesse M, Tchelepi HA, and Orr FM (2006) Onset of convection in a gravitationally unstable diffusive boundary layer in porous media. *J. Fluid Mech.* 548, 87.
11. Hesse MA, Tchelepi HA, and Orr FM (2006) Natural convection during aquifer CO₂ storage, In the 8th International Conference on Greenhouse Gas Control Technologies. Trondheim, Norway.
12. Wooding RA (1969) Growth of fingers at an unstable diffusing interface in a porous medium or Hele-Shaw cell. *J. Fluid Mech.* 39, 477.
13. Kneafsey TJ and Pruess K (2010) Laboratory flow experiments for visualizing carbon dioxide-induced, density-driven brine convection. *Transport in Porous Media* 82, 123.
14. Neufeld JA, Hesse MA, Riaz A, Hallworth MA, Tchelepi HA, and Huppert HE (2010) Convective dissolution of carbon dioxide in saline aquifers. *Geophys. Res. Lett.* 37, L22404.
15. Backhaus S, Turitsyn K, Ecke R (2011) Convective instability and mass transport of diffusion layers in a Hele-Shaw geometry. *Phys. Rev. Lett.* 106, 104501.
16. MacMinn CW, Neufeld JA, Hesse MA, Huppert HE (2012) Spreading and convective dissolution of carbon dioxide in vertically confined, horizontal aquifers. *Water Resour. Res.* 48, W11516.
17. Robinson JL (1976) Theoretical analysis of convective instability of a growing horizontal thermal boundary layer. *Phys. Fluids* 19, 778.
18. Woods AW, Espie T (2012) Controls on the dissolution of CO₂ plumes in structural traps in deep saline aquifers. *Geophys. Res. Lett.* 39, L08401.

19. Hassanzadeh H, Pooladi-Darvish M and Keith DW (2007) Scaling behavior of convective mixing, with application to geological storage of CO₂. *AIChE Journal* 53, 1121.
20. Rees DAS, Selim A, and Ennis-King JP (2008) The instability of unsteady boundary layers in porous media. In *Emerging Topics in Heat and Mass Transfer in Porous Media From Bioengineering and Microelectronics to Nanotechnology*, edited by P. Vadasz (Springer Netherlands).
21. Hidalgo JJ and Carrera J (2009) Effect of dispersion on the onset of convection during CO₂ sequestration. *J. Fluid Mech.* 640, 441.
22. Pau GSH, Bell JB, Pruess K, Almgren AS, Lijewski MJ, Zhang K (2010) High-resolution simulation and characterization of density-driven flow in CO₂ storage in saline aquifers. *Advances in Water Resources* 33, 443-455.
23. Bachu S, Gunter WD, and Perkins EH (1994) Aquifer disposal of CO₂ - Hydrodynamic and mineral trapping, *Energy Convers. Manage.* 35:269–279.
24. Ennis-King J and Paterson L (2007) Coupling of geochemical reactions and convective mixing in the long-term geological storage of carbon dioxide. In the 8th International Conference on Greenhouse Gas Control Technologies, Trondheim, Norway, 2006. Proceedings edited by J. Gale and O. Bolland (Elsevier Sci Ltd, Oxford).
25. Andres JTH and Cardoso SSS (2011) Onset of convection in a porous medium in the presence of chemical reaction. *Phys. Rev. E* 83, 046312.
26. Ghesmat K, Hassanzadeh H, and Abedi J (2011) The impact of geochemistry on convective mixing in a gravitationally unstable diffusive boundary layer in porous media: CO₂ storage in saline aquifers. *J. Fluid Mech.* 673, 480.
27. Andres JTH and Cardoso SSS (2012) Convection and reaction in a diffusive layer in a porous medium. *CHAOS* 22, 037113.
28. CSIRO (2000) *Fastflo Tutorial Guide (version 3)*, (CSIRO, Australia).
29. Eckert K and Grahn A (1999) Plume and finger regimes driven by an exothermic interfacial reaction, *Phys. Rev. Lett.* 82 (22), 4436.
30. Eckert K, Acker M, and Shi Y (2004) Chemical pattern formation driven by a neutralization reaction. I. Mechanism and basic features. *Phys. Fluids* 16 (2), 385.
31. Almarcha C, Trevelyan PMJ, Grosfils P and De Wit A (2010a) Chemically driven hydrodynamic instabilities. *Phys. Rev. Lett.* 104 (4), 269.
32. Almarcha C, Trevelyan PMJ, Riolfo LA, Zalts A, El Hasi C, D'Onofrio A and De Wit A (2010b) Active Role of a Color Indicator in Buoyancy-Driven Instabilities of Chemical Fronts. *J. Phys. Chem. Lett.* 1 (4), 752.
33. Kuster S, Riolfo LA, Zalts A, El Hasi C, Almarcha C, Trevelyan PMJ, De Wit A and D'Onofrio A (2011) Differential diffusion effects on buoyancy-driven instabilities of acid-base fronts: the case of a color indicator. *Phys. Chem. Chem. Phys.* 13, 17295.

34. Bratsun D A and De Wit A (2011) Buoyancy-driven pattern formation in reactive immiscible two-layer systems. *Chem. Eng. Sci.* 66 (22), 5723.
35. Wittke G (1983) Reactions of phenolphthalein at various pH values. *J. Chem. Ed.* 60, 3.
36. Nicholson L (1989) Kinetics of the fading of phenolphthalein in alkaline solution. *J. Chem. Ed.* 66, 725.
37. Homsy GM (1987) Viscous Fingering in Porous Media. *Annu. Rev. Fluid Mech.* 19, 271.
38. Lay T, Herndlund J, Buffett BA (2008) Core–mantle boundary heat flow. *Nature Geoscience* 1: 25.
39. Holzbecher E (1998) *Modeling Density-Driven Flow in Porous Media* (Springer-Verlag, Berlin).

FIGURE LEGENDS

FIG. 1. Sketch of carbon dioxide sequestration in a saline aquifer. Minerals M_1 and M_2 are, e.g., calcium feldspar and calcite, respectively.

FIG. 2. (Color online) Effect of reaction strength (Da/Ra^2) on the marginal stability curve ($\sigma = 0$) in the transverse wavenumber k – time t domain.

FIG. 3. (Color online) Evolution of the maximum growth rate σ_{\max} and most unstable wavenumber k_{\max} for different reaction strengths.

FIGURE 4. (Color online) Sequence of photographs showing the evolution of the pink diffusive boundary layer formed by the reaction of phenolphthalein in MIBK (top layer) with aqueous sodium hydroxide (bottom layer) in a Hele-Shaw cell. Reaction strength increases from cases A to C. The lengthscale unit is centimetre.

FIG. 5. (Color online) Effects of reaction strength Da/Ra^2 on times for onset and cessation of convection (solid line) as well as on the maximum growth rate $\sigma_{\max kt}$ (dotted line) predicted from linear stability analysis. Experimental measurements of times for onset and cessation of convection for the reactive (diamonds) and inert (circle) systems are also shown.

(FIGURES AND FIGURE LEGENDS)

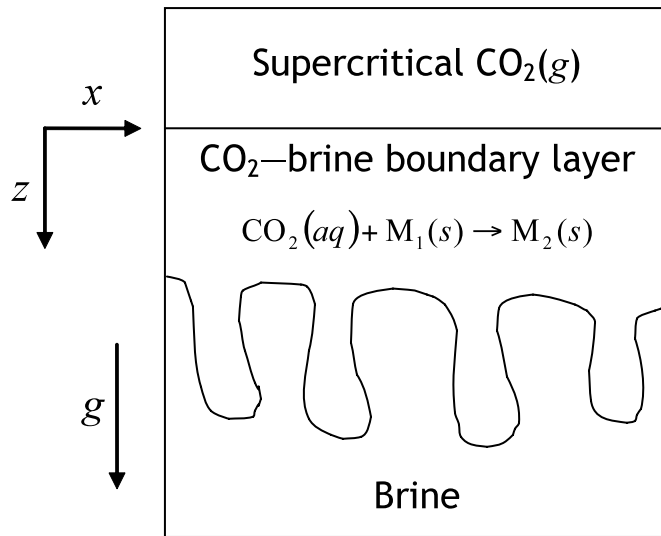


FIG. 1. Sketch of carbon dioxide sequestration in a saline aquifer. Minerals M_1 and M_2 are, e.g., calcium feldspar and calcite, respectively.

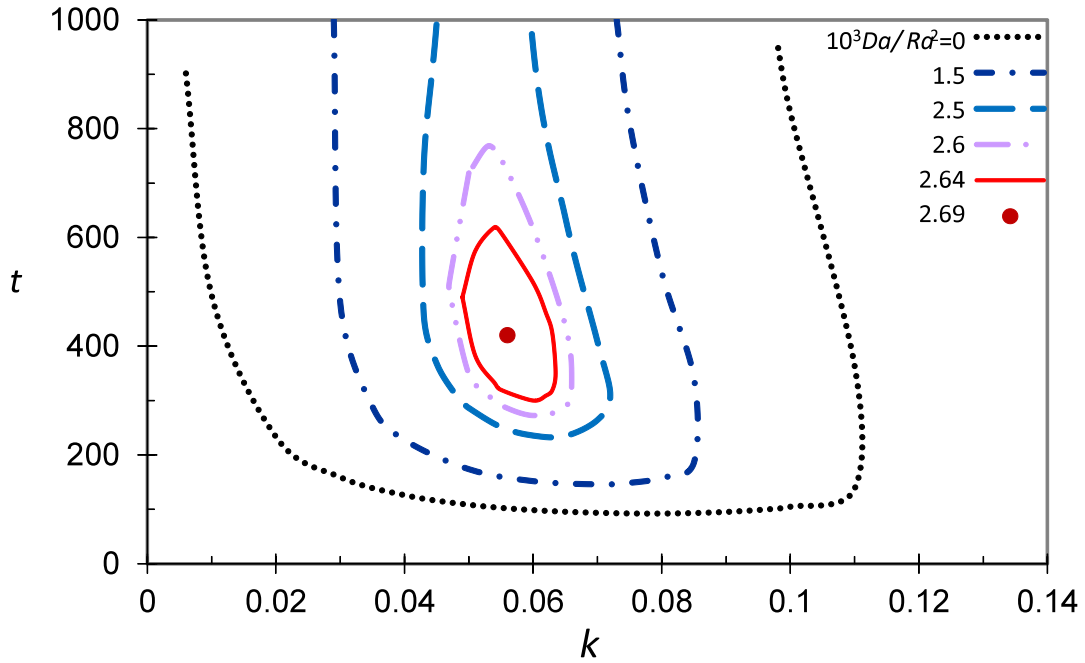


FIG. 2. (Color online) Effect of reaction strength (Da/Ra^2) on the marginal stability curve ($\sigma = 0$) in the transverse wavenumber k – time t domain.

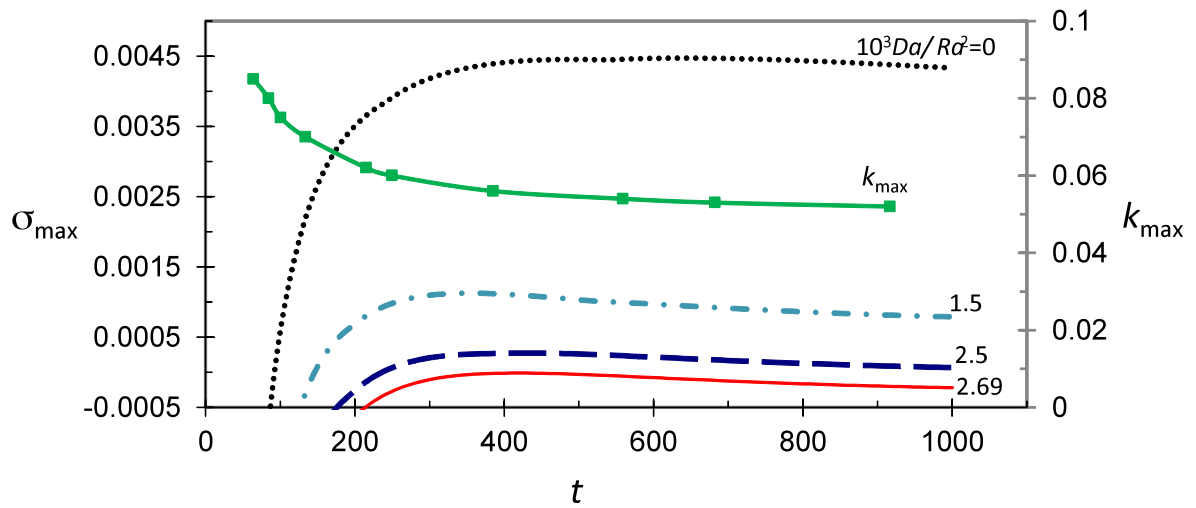


FIG. 3. (Color online) Evolution of the maximum growth rate σ_{\max} and most unstable wavenumber k_{\max} for different reaction strengths.

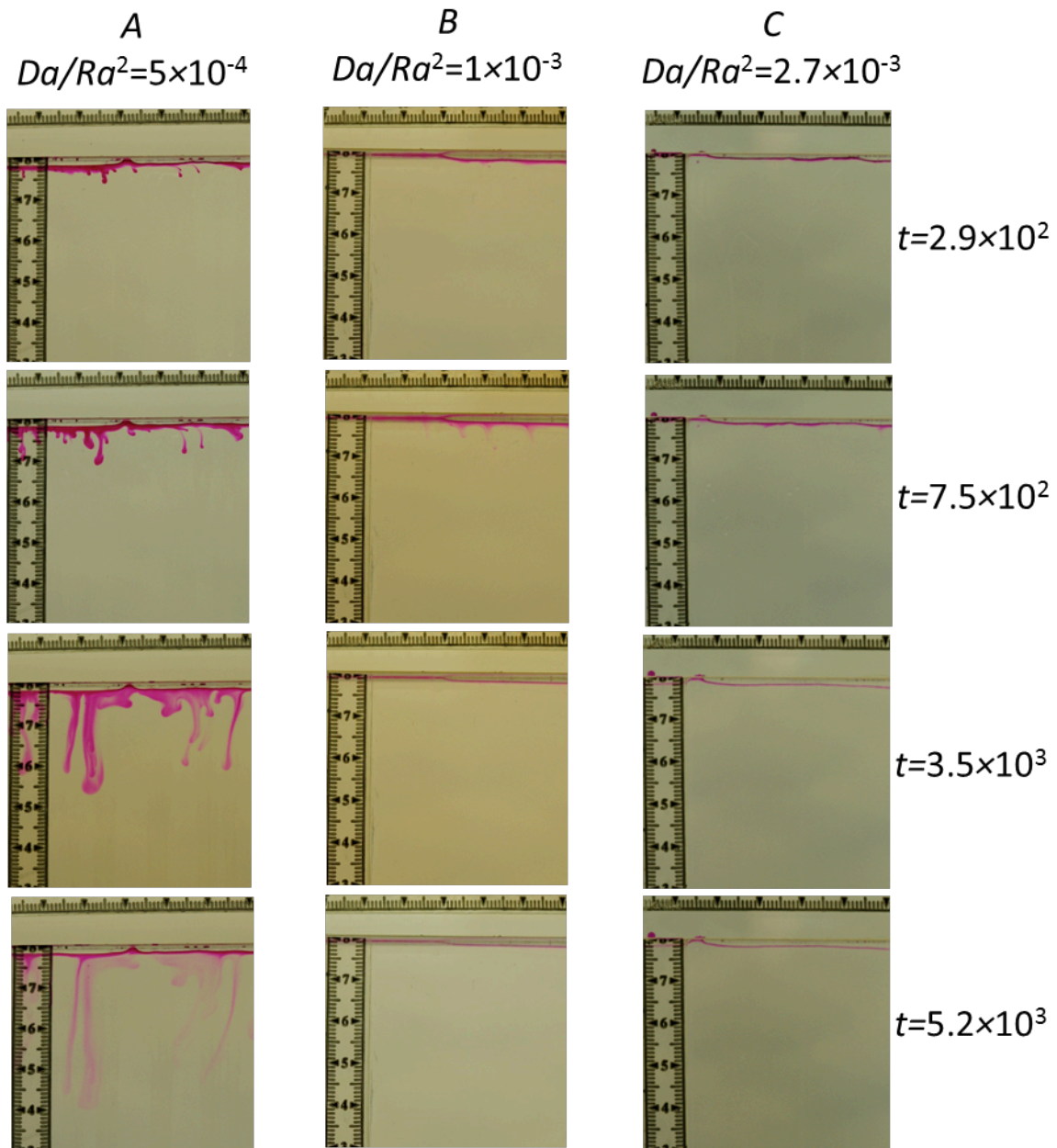


FIGURE 4. (Color online) Sequence of photographs showing the evolution of the pink diffusive boundary layer formed by the reaction of phenolphthalein in MIBK (top layer) with aqueous sodium hydroxide (bottom layer) in a Hele-Shaw cell. Reaction strength increases from cases A to C. The lengthscale unit is centimetre.

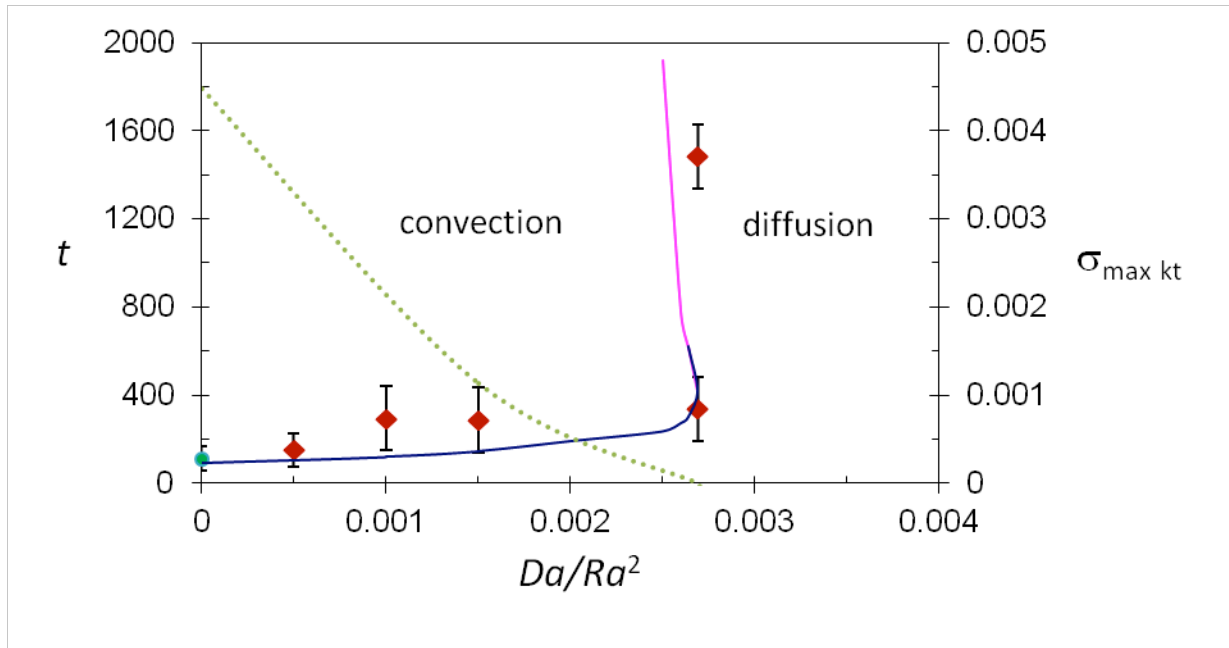


FIG. 5. (Color online) Effects of reaction strength Da/Ra^2 on times for onset and cessation of convection (solid line) as well as on the maximum growth rate $\sigma_{\max kt}$ (dotted line) predicted from linear stability analysis. Experimental measurements of times for onset and cessation of convection for the reactive (diamonds) and inert (circle) systems are also shown.